First-principles study of the ferroelectric Aurivillius phase Bi_2WO_6

Hania Djani,[1,2,*] Eric Bousquet,[3,4] Abdelhafid Kellou,[2] and Philippe Ghosez[3]
[1]*Centre de Développement des Technologies Avancées, Cité 20 Aout 1956, Baba Hassen, Alger, Algeria*
[2]*Faculté de Physique, USTHB, B.P. 32 El Alia, Bab Ezzouar, 16111 Alger, Algeria*
[3]*Physique Théorique des Matériaux, Université de Liège (B5), B 4000 Liège, Belgium*
[4]*Department of Materials, ETH Zurich, Wolfgang-Pauli-Strasse 27, CH 8093 Zurich, Switzerland*
(Received 4 April 2012; published 8 August 2012)

In order to better understand the reconstructive ferroelectric-paraelectric transition of Bi_2WO_6, which is unusual within the Aurivillius family of compounds, we performed first-principles calculations of the dielectric and dynamical properties of two possible high-temperature paraelectric structures—the monoclinic phase of $A2/m$ symmetry observed experimentally and the tetragonal phase of $I4/mmm$ symmetry—common to most Aurivillius-phase components. Both paraelectric structures exhibit various unstable modes, which, after their condensation, bring the system toward more stable structures of lower symmetry. The calculations confirm that, starting from the paraelectric $A2/m$ phase at high temperatures, the system must undergo a reconstructive transition to reach the $P2_1ab$ ferroelectric ground state.

DOI: 10.1103/PhysRevB.86.054107 PACS number(s): 77.80.−e, 77.84.Bw, 71.15.Mb, 63.22.Np

I. INTRODUCTION

The Aurivillius phases constitute a family of naturally occurring, complex, layered oxide structures in which fluorite-like $(Bi_2O_2)^{+2}$ units alternate with perovskite-like $(A_{m-1}B_mO_{3m+1})^{-2}$ blocks, where A = Ca^{+2}, Ba^{+2}, Sr^{+2}, Bi^{+2}, etc., B = Fe^{+3}, Ti^{+4}, Nb^{+5}, Ta^{+5}, W^{+6}, etc., and m is the number of BO_6 octahedra in the perovskite-like blocks (m = 1–8).[1] The oxidation states of the cations and m are interdependent, to always provide the right number of electrons to oxygen atoms. This family has numerous representatives, the most studied being Bi_2WO_6 (m = 1), $SrBi_2Ta_2O_9$ (m = 2), and $Bi_4Ti_3O_{12}$ (m = 3).[2–6] The ferroelectric properties of the Aurivillius phases have been widely studied since the early works of Subbarao[7] and Smolenskii *et al.*[8] and they continue to rise technological interest mainly for their potential use in thin film nonvolatile memory applications.[9] They are also attractive at the fundamental level because of the peculiarity of their phase transitions and the complex interplay of their structural instabilities.

Bi_2WO_6 is the simplest member of the Aurivillius family, with one oxygen octahedron sandwiched between two Bi_2O_2 layers. It possesses many interesting physical properties such as ferroelectricity with large spontaneous polarization and a high Curie temperature (950°C), piezoelectricity with a potential for high-frequency and high-temperature applications as an alternative to $BaTiO_3$ and $PbZr_{1-x}Ti_xO_3$,[10] a high ion conductivity,[11] and photocatalytic activity.[12]

Understanding ferroelectricity and the sequence of phase transitions in this compound is still challenging. Experimental studies[13] showed that Bi_2WO_6 is polar at ambient temperature, with an orthorhombic $P2_1ab$ (No. 29) structure. Increasing the temperature reveals, at 670°C, a transition to an intermediate polar phase with an orthorhombic $B2cb$ (No. 41) structure. This structure is maintained until 950°C, then the material displays a transition to a paraelectric monoclinic $A2/m$ (No. 12) structure. This type of ferroelectric-paraelectric transition to an $A2/m$ phase is unexpected and rather unique among Aurivillius phases, where usually compounds transform at high temperatures into a centrosymmetric tetragonal $I4/mmm$ (No. 139) structure.[6] The same kind of behavior appears in Bi_2MoO_6, a compound isomorphic to Bi_2WO_6, which exhibits orthorhombic structures at low and intermediate temperatures and a monoclinic $P2_1/c$ (No. 14) structure at high temperature.[14,15] Such ferroelectric to paraelectric transitions from orthorhombic to monoclinic are necessarily reconstructive since the space groups of the low temperature phases are not subgroups of the high temperature phases ($A2/m$ or $P2_1/c$), but rather of the $I4/mmm$ structure.

We performed first-principles calculations in order to better understand these intriguing observations. First-principles studies of Bi_2WO_6 have been reported in the literature previously. Machado *et al.*[16] performed frozen-phonon calculations of the polar modes at the Brillouin-zone center in the hypothetical $I4/mmm$ tetragonal paraelectric phase in order to clarify the microscopic origin of the ferroelectric instability. More recently, Mohn and Stolen[17] highlighted the modification of the oxygen arrangement around Bi atoms in Bi_2O_2 layers at the reconstructive ferroelectric-paraelectric transition. In the present work, we complete these studies by reporting a systematic investigation of the structural, dielectric, and dynamical properties of both potential high-temperature $A2/m$ and $I4/mmm$ paraelectric phases. We investigate the energy landscape around these two phases. The structure and internal energy of various other intermediate phases, reached by the condensation of individual or combined lattice instabilities at the zone center and zone boundaries of the Brillouin zone, are calculated. A diagram comparing the internal energies of various possible phases is then established, which confirms that, starting from the high-temperature paraelectric $A2/m$ phase, the system must undergo, upon cooling, a reconstructive phase transition to reach the $P2_1ab$ ground-state structure. Spontaneous polarizations of different polar phases are also reported.

II. TECHNICALITIES

The calculations were performed within density functional theory,[18,19] using a plane-wave pseudopotentials method thanks to the ABINIT package.[20–22] The exchange-correlation

energy functional was evaluated within the local density approximation (LDA) as parameterized by Perdew and Wang.[23] Extended norm-conserving pseudopotentials from Teter[24] were used, with Bi($5d$ $6s6p$), W($5s$ $5p$ $5d$ $6s$), and O($2s$ 2p) levels treated as valence states. Wave functions were expanded up to a kinetic energy cutoff of 50 Hartrees. Integrals over the Brillouin zone were approximated by sums on a $6 \times 6 \times 1$ Monkhorst-Pack mesh of special k points.[25] The structural optimization was done using the Broyden-Fletcher-Goldfarb-Shanno minimization algorithm.[26] We calculated the *ab initio* forces on the ions and relaxed the position of each individual atom until the absolute values of the forces were converged to less than 10^{-5} Ha/Bohr. Phonons, Born effective charges and dielectric tensors were calculated using density functional perturbation theory,[27] and spontaneous polarization using the Berry phase formalism.[29]

III. HIGH-TEMPERATURE $A2/m$ MONOCLINIC STRUCTURE

We begin our study by fully characterizing the experimentally observed paraelectric $A2/m$ phase. In this structure, for the first time, phonon instabilities are calculated together with dielectric properties and Born effective charges. Further, we move on with the characterization of the hypothetical paraelectric $I4/mmm$ phase.

A. Structure

The monoclinic $A2/m$ paraelectric phase of Bi_2WO_6 (conventionally $C2/m$) contains 2 formula units per primitive unit cell (18 atoms). The structure, illustrated in Fig. 1, consists of alternative Bi_2O_2 fluorite-like and WO_4 layers. Within this structure the oxygen octahedra exhibit a peculiar edge-sharing along the a axis. Along the b axis, the oxygen octahedra are corner-sharing. As is conventional for Aurivillius phases, the stacking axis normal to the layers is defined as the c axis of the $A2/m$ structure. The calculated lattice parameters and internal positions are listed in Table I. Except for the systematic LDA underestimate of lattice parameters, the results are in reasonable agreement with the experiment. We note that the lattice constants of Mohn and Stolen[17] within the generalized gradient approximation (GGA) are in closer agreement with the experiment. This might, however, be partly fortuitous: contrary to the LDA, the GGA is well known to overestimate lattice constants, and this typical error (observed in the lower temperature $B2cb$ phase, as discussed in the next section) might be partly compensated here by the thermal expansion, since the experimental results to which the zero-temperature calculations are compared were done at 965°C.

B. Dielectric properties

Study of the Born effective charges (Z^*) and optical dielectric tensor (ε_∞) is important for the identification of the long-range dipolar contribution to the lattice dynamic of a polar insulator. Our results for Z^* of nonequivalent atoms are presented in Table II. For clarity, we note that $A2/m$ has its a and b axes aligned along the Cartesian x and y directions, respectively, and the c axis makes an angle of $(\beta - \frac{\pi}{2})$ with the z direction. Within this choice of Cartesian axis, the Born

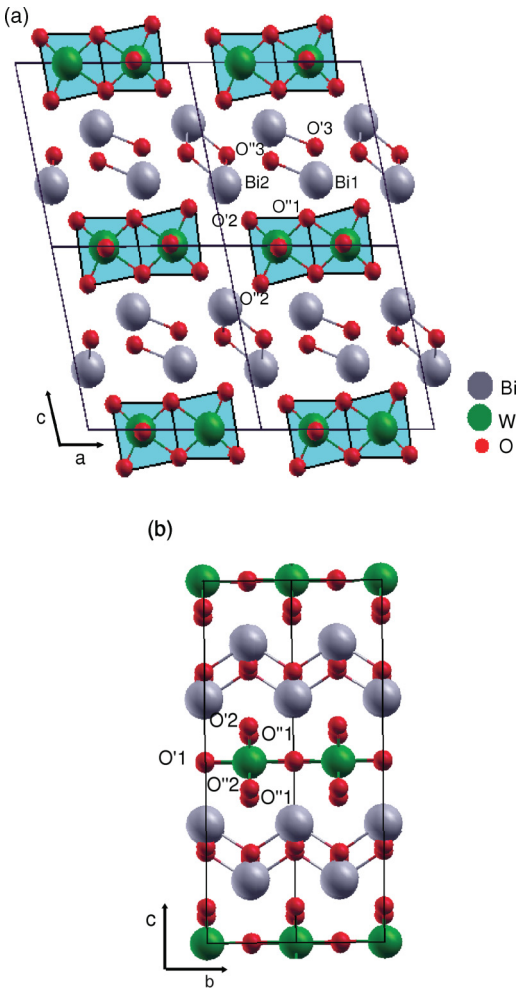

FIG. 1. (Color online) Monoclinic $A2/m$ paraelectric phase of Bi_2WO_6 showing (a) edge-sharing octahedra in the ac plane and (b) corner-sharing octahedra in the bc plane.

effective charge tensor has the form

$$Z^* = \begin{pmatrix} Z^*_{xx} & 0 & Z^*_{xz} \\ 0 & Z^*_{yy} & 0 \\ Z^*_{zx} & 0 & Z^*_{zz} \end{pmatrix}.$$

The Born effective charges for this material are much larger than the nominal ionic ones and so follow the tendency observed for the class of perovskite ABO_3 compounds.[30] Giant anomalous Z^* values are observed on W ($+10.5e$) and O'_1 ($-7.76e$) belonging to the W-O'_1 chains aligned along the b axis. These values are similar to those reported for WO_3[31] and can be assigned to W $5d$–O $2p$ dynamical changes of hybridization. Anomalous parts of the charge on W, and on its surrounding O''_1, O'_2, and O''_2 oxygen atoms, are strongly reduced along the x and z directions where W-O chains are broken. Anomalous Z^* values are also observed in the Bi_2O_2 layer, with a large contribution observed on Bi and its surrounding oxygen atoms. One can see a significant difference between Bi_1 and Bi_2 (in the x direction) despite their apparently similar environments in the Bi_2O_2 layer. The Born effective charge is known to be a sensitive tool for probing covalency effects[30] and our results therefore support the recent

TABLE I. Calculated cell parameters and internal atomic positions in the paraelectric $A2/m$ phase of Bi_2WO_6. Experimental values from Ref. 13 are reported in parentheses for comparison.

	Atom	Wyckoff	x	y	z
$a = 8.11$ Å	Bi_1	$4i$	0.9307	0.0000	0.1588
(8.37)			(0.9310	0.0000	0.1640)
	Bi_2	$4i$	0.3905	0.0000	0.1756
$b = 3.75$ Å			(0.3950	0.0000	0.1768)
(3.85)	W	$4i$	0.2979	0.5000	0.0000
			(0.3007	0.5000	0.0000)
$c = 15.90$ Å	O'_1	$4i$	0.3142	0.0000	0.0024
(16.44)			(0.3113	0.0000	0.0035)
	O''_1	$4i$	0.5090	0.5000	−0.0811
$\beta = 102.12°$			(0.5080	0.5000	−0.0770)
(102.33)	O'_2	$4i$	0.1638	0.5000	−0.0736
			(0.1734	0.5000	−0.0710)
	O''_2	$4i$	0.1661	0.5000	0.1059
			(0.1640	0.5000	0.1009)
	O'_3	$4i$	0.1172	0.0000	0.2500
			(0.1170	0.0000	0.2512)
	O''_3	$4i$	0.3618	0.5000	0.2660
			(0.3638	0.5000	0.2668)

work by Mohn *et al.*[17] who suggest that the local environment around Bi is asymmetric, with Bi_1 and Bi_2 forming different numbers of bonds with the apex oxygen of the perovskite layer.

Finally, the optical dielectric constant is computed:

$$\varepsilon_\infty = \begin{pmatrix} 6.49 & 0 & 0.08 \\ 0 & 7.25 & 0 \\ 0.08 & 0 & 6.37 \end{pmatrix}.$$

We have no experimental values to compare with and our prediction must be considered an upper bound, because of the typical LDA overestimation of ε_∞.

C. Phonon instabilities

Phonon calculations were performed to study the structural stability of the $A2/m$ monoclinic configuration. Zone-center phonons were computed in the conventional cell of 36 atoms, with the primitive cell doubled along the b axis. Due to the folding of the Brillouin zone, this gives access to phonons at Γ and V. The full list of Γ frequencies is reported in the Appendix for completeness. The system reveals four instable modes: two at Γ, with frequencies at $108i$ and $63i$ cm^{-1}, corresponding to the irreducible representation labels[32] Γ_1^- and Γ_2^+, respectively; and two others at the zone-boundary point $V = (0,1/2,0)$, with frequencies at $89i$ and $65i$ cm^{-1}, corresponding to V_1^- and V_1^+, respectively. The strongest unstable mode, Γ_1^-, is polar along the b axis. In Table III, where real-space eigendisplacements of these unstable modes are listed, we can see that all of them restrict their atomic motions along the b-axis direction only and that, contrary to what is usually observed in other paraelectric Aurivillius phases, the $A2/m$ monoclinic configuration is not unstable against oxygen octahedron rotational modes, which are prevented by the edge-sharing spatial organization.

Unstable modes were then individually condensed into the $A2/m$ phase and each of the lower symmetry phases reached under these condensations is fully relaxed. From the results reported in Table IV, we can see that the condensation of the polar unstable mode Γ_1^- into $A2/m$ leads to a ferroelectric phase with a monoclinic $A2$ (No. 5) structure, while the condensation of V_1^-, V_1^+, and Γ_2^+ lead to a monoclinic $P\bar{1}$ (No. 2) structure. After full relaxation, these phases exhibit nearly identical cell parameters and total energy values close to each others'. The lowest energy configuration corresponds to the monoclinic $P\bar{1}$ phase arising from the condensation of V_1^+ with a decrease in energy, with respect to the $A2/m$ phase, of 9.25 meV/formula unit. Further phonon calculations in this phase do not reveal any unstable mode, identifying it as a potential ground state.

TABLE II. Nonzero elements of the calculated Born effective charge tensors in Cartesian coordinates (see text) for Bi_2WO_6 in the monoclinic $A2/m$ phase. The nominal charge of each atom (Z_{nom}) is reported for comparison.

Atom	Z^*_{xx}	Z^*_{yy}	Z^*_{zz}	Z^*_{xz}	Z^*_{zx}	Z_{nom}
Bi_1	5.34	5.38	4.35	0.24	−0.36	+3
Bi_2	4.37	5.17	4.53	−0.18	0.18	+3
W	6.58	10.5	7.33	0.08	0.63	+6
O'_1	−1.21	−7.76	−1.34	−0.01	−0.06	−2
O''_1	−3.27	−2.68	−3.33	−0.75	−0.91	−2
O'_2	−2.73	−2.18	−2.71	2.00	2.02	−2
O''_2	−2.34	−2.5	−3.86	−1.33	−1.44	−2
O'_3	−3.25	−2.97	−2.68	−0.21	0.04	−2
O''_3	−3.46	−2.96	−2.27	0.16	−0.10	−2

D. Spontaneous polarization

As highlighted in the previous section, starting from the $A2/m$ phase, a ferroelectric $A2$ structure can be reached from the condensation of an unstable Γ_1^- mode, giving rise to a polarization along the b direction. The amplitude of this polarization can be computed using the Berry phase formalism but requires caution.

Indeed, the modern theory of polarization (see, e.g., Ref. 29) teaches us that the spontaneous polarization P_s of the ferroelectric $A2$ structure is related to the *formal* polarizations of the ferroelectric (P_{A2}) and paraelectric ($P_{A2/m}$) phases by

$$P_s = P_{A2} - P_{A2/m} + n|P_Q|, \tag{1}$$

where n is an integer and $P_Q = 2e\mathbf{R}/\Omega$ is the so-called polarization quantum, with $\mathbf{R}$ the shortest lattice vector along the polarization direction and Ω the unit-cell volume. The factor of 2 accounts for the double band occupancy.

From Eq. (1), the determination of P_s from only knowledge of the formal polarizations P_{A2} and $P_{A2/m}$ is possible only modulo P_Q. This quantum indeterminancy arises from the fact that the formal polarizations of the P_{A2} and $P_{A2/m}$ phases are themselves defined only modulo P_Q so that the value of P_s depends on the specific choice of a polarization branch (i.e., choice of how we connect a given $P_{A2/m}$ point on the left to a given P_{A2} point on the right in Fig. 2). Of course, P_s is a well-defined quantity but its unambiguous determination additionally requires us to determine n through

TABLE III. Real-space eigendisplacements η of unstable phonon modes of the $A2/m$ structure. Eigendisplacements are normalized within the 36-atom cell according to $\langle\eta|M|\eta\rangle = 1$, with the mass matrix M in atomic mass units.[28] Internal coordinates of the atoms of the $A2/m$ phase are those presented in Table I. Mode frequencies, in brackets, are in cm^{-1}.

	η											
	Γ_1^- [108i]			V_1^- [89i]			V_1^+ [65i]			Γ_2^+ [63i]		
Atom	x	y	z	x	y	z	x	y	z	x	y	z
Bi_1	0.000	−0.001	0.000	0.000	0.006	0.000	0.000	0.004	0.000	0.000	0.003	0.000
Bi_2	0.000	0.000	0.000	0.000	0.004	0.000	0.000	0.007	0.000	0.000	0.004	0.000
W	0.000	0.021	0.000	0.000	0.027	0.000	0.000	0.035	0.000	0.000	0.036	0.000
O_1'	0.000	−0.032	0.000	0.000	−0.023	0.000	0.000	0.002	0.000	0.000	0.003	0.000
O_1''	0.000	−0.045	0.000	0.000	−0.037	0.000	0.000	−0.012	0.000	0.000	−0.007	0.000
O_2'	0.000	−0.044	0.000	0.000	−0.034	0.000	0.000	−0.005	0.000	0.000	−0.022	0.000
O_2''	0.000	−0.067	0.000	0.000	−0.055	0.000	0.000	−0.024	0.000	0.000	−0.022	0.000
O_3'	0.000	−0.022	0.000	0.000	0.002	0.000	0.000	−0.002	0.000	0.000	−0.002	0.000
O_3''	0.000	−0.020	0.000	0.000	−0.012	0.000	0.000	0.006	0.000	0.000	0.001	0.000

proper integration of the polarization current along an adiabatic insulating path between the paraelectric and the ferroelectric phases.

When the polarization quantum is large compared to the spontaneous polarization, as in conventional ABO_3 compounds, the uncertainty can be easily fixed. But in materials like Aurivillius compounds that have large unit cells, the quantum is small and potentially of the same order of magnitude as the spontaneous polarization (in the present case $P_Q = 25.90\ \mu C/cm^2$), and getting rid of the quantum indeterminancy requires us to follow the evolution of the polarization along the atomic distortion from the paraelectric to the ferroelectric phase. In practice, this can be achieved by computing the formal polarizations of intermediate structures as illustrated in Fig. 2. The choice of the appropriate branch (solid lines in the graph) becomes obvious when the change in polarization from one intermediate structure to the next one is small compared to the polarization quantum. From this, we deduce that the spontaneous polarization of the $A2$ phase is $P_s = 20.02\ \mu C/cm^2$. We note that this value differs significantly from the one that would have been naively deduced from the difference between the values of the formal polarizations in the interval $[-P_Q/2, P_Q/2]$, as typically delivered in the output of conventional first-principles software (i.e., $P_{A2} = -5.88\ \mu C/cm^2$ and $P_{A2/m} = 0\ \mu C/cm^2$, yielding $P_s = -5.88\ \mu C/cm^2$).

Alternatively, it is also possible to estimate the polarization from knowledge of the Born effective charges and atomic displacements using the expression

$$P_{s,\alpha} = \frac{e}{\Omega} \sum_{\kappa,\beta} Z^*_{\kappa,\alpha\beta} \delta\tau_{\kappa,\beta}, \tag{2}$$

where $\delta\tau_{\kappa,\beta}$ is the displacement of atom κ along direction β from the paraelectric to the ferroelectric phase, and $Z^*_{\kappa,\alpha\beta}$ the Born effective charge tensor of atom κ. This provides $P_s = 20.73\ \mu C/cm^2$, in close agreement with the Berry phase estimate and coherent with the quasilinear evolution of the polarization with the structural distortion shown in Fig. 2. We note that Eq. (2) gives access to the slope at the origin of the appropriate polarization branch in Fig. 2 and provides an easy alternative way to identify it.

IV. HYPOTHETICAL HIGH-TEMPERATURE *I*4/*mmm* TETRAGONAL STRUCTURE

Starting at a high temperature, from the experimentally observed paraelectric $A2/m$ structure, one would anticipate,

TABLE IV. Cell parameters (lengths in Å and angles in degrees) and difference in energies ΔE_m with respect to the paraelectric monoclinic $A/2m$ phase (in meV/formula unit) after full atomic relaxation of the different phases reached by the condensation of individual unstable phonon modes in the $A/2m$ phase. The label and frequency ω (in cm^{-1}) of the mode that was initially condensed, together with the symmetry of the related phase, are also listed.

Mode	ω	Symmetry	Cell parameters	ΔE_m
Γ_1^-	108i (polar)	$A2$	$a = 8.09, b = 3.77, c = 15.87$ $\alpha = 90°, \beta = 101.50°, \gamma = 90°$	−7.82
V_1^-	89i	$P\bar{1}$	$a = 8.09, b = 3.77, c = 15.88$ $\alpha = 90.00°, \beta = 101.50°, \gamma = 89.99°$	−6.87
V_1^+	65i	$P\bar{1}$	$a = 8.09, b = 3.77, c = 15.87$ $\alpha = 89.99°, \beta = 101.50°, \gamma = 89.99°$	−9.25
Γ_2^+	63i	$P\bar{1}$	$a = 8.09, b = 3.77, c = 15.87$ $\alpha = 90.30°, \beta = 101.50°, \gamma = 90.10°$	−8.16

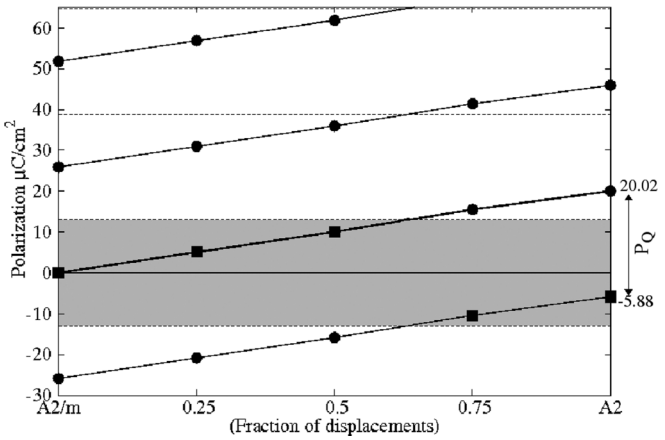

FIG. 2. Change in polarization p along a path of atomic distortions from the paraelectric $A2/m$ structure to the ferroelectric $A2$ structure. The possible values of P at given atomic positions differ by multiples of the polarization quantum, $P_Q = 25.90\,\mu\text{C/cm}^2$. Squares represent formal polarizations in the interval $[-P_Q/2, P_Q/2]$ (gray area).

from the previous discussion, a transition to a nonferroelectric $P\bar{1}$ ground state. Instead, experiments show that Bi_2WO_6 exhibits low-temperature phases of orthorhombic $B2cb$ and $P2_1ab$ symmetries, subgroups of the centrosymmetric $I4/mmm$ parent phase, that is, the high-temperature paraelectric phase of all Aurivillius compounds with a number of perovskite blocks $m > 1$. We thus continue our study by considering the hypothetical $I4/mmm$ paraelectric phase.

A. Structure

The $I4/mmm$ structure as illustrated in Fig. 3(a) contains 2 formula units per primitive unit cell (18 atoms) and consists of Bi_2O_2 fluorite-like layers alternating with perovskite-like blocks of corner-sharing octahedral chains. Since $I4/mmm$ is not observed experimentally, an estimate of the paraelectric unit cell is deduced from the orthorhombic lattice parameters of the experimental ferroelectric phase cited in Ref. 16, using $a_{\text{tetra}} = b_{\text{tetra}} = 3.86$ Å $= \sqrt{a_{\text{orth}} b_{\text{orth}}/2})$ and $c_{\text{tetra}} = 16.52$ Å. In order to facilitate the comparison with the experimentally observed orthorhombic ferroelectric ground state, which contains 4 formula units per primitive unit cell (36 atoms), our calculations were performed in a tetragonal $I4/mmm$ unit cell doubled along the [110] directions, where the lattice parameters become $a = b = 5.45$ Å, $c = 16.52$ Å [see Fig. 3(b)], allowing the paraelectric and ferroelectric phases to have the same number of atoms and the same orientation. In what follows, a, b, and c are the vectors of our doubled unit cell so that the a and b directions refer to the [110] directions of the conventional centered unit cell, and c to the direction perpendicular to them.

Structural parameters and internal atomic positions of the $I4/mmm$ hypothetical structure after full atomic relaxation are reported in the top part of Table V. Our internal coordinates show good agreement with those calculated by Machado *et al.* in Ref. 16; those authors, however, worked with larger lattice

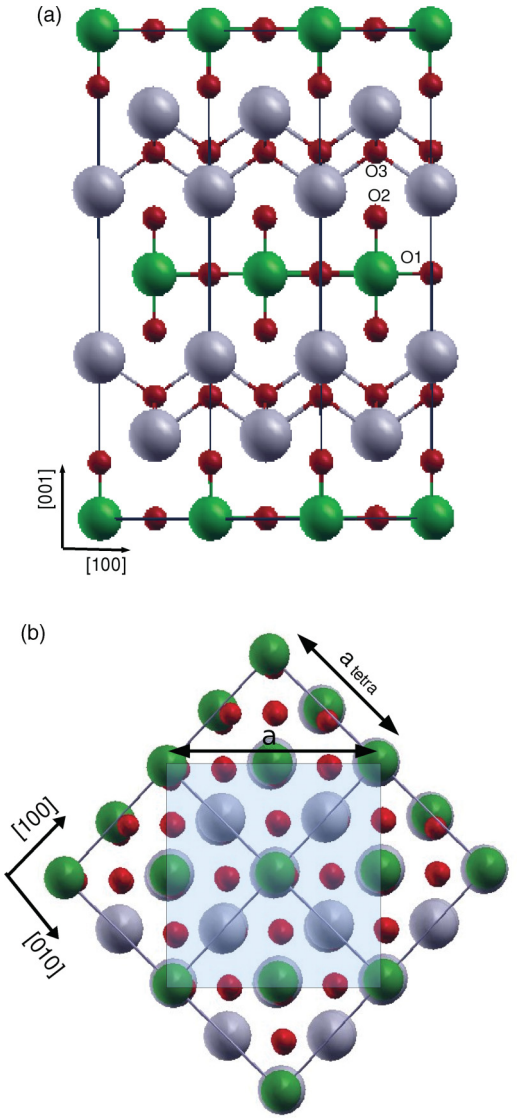

FIG. 3. (Color online) The hypothetical tetragonal $I4/mmm$ paraelectric phase of Bi_2WO_6: (a) side view and (b) top view, highlighting the corresponding doubled cell in the [110] direction.

constants, corresponding to experimental values estimated as discussed above.

We further note that the internal energy of the relaxed $I4/mmm$ structure is 156 meV per formula unit higher than that of the $A2/m$ phase. Henceforth, we report the energies taking the $I4/mmm$ structure as the reference. A summary of the internal energies of all phases studied is provided in Sec. V.

B. Dielectric properties

Our results for the dynamical effective charges of Bi_2WO_6 in the $I4/mmm$ phase, for nonequivalent atoms, are presented in Table VI. In this case, the Cartesian x, y, and z axes are aligned along the crystalline a, b, and c directions.

As expected, there are large anomalous contributions to Z^*, on W$(+11e)$ and $O_1(-4.88e)$ atoms in the octahedral ab plane and on W$(+9.32e)$ and $O_2(-4.74e)$ atoms in the apical direction. Within Bi_2O_2 layers, the large charges also

TABLE V. Calculated unit cell parameters and internal atomic positions in the hypothetical paraelectric $I4/mmm$ phase doubled along [110] and the $B2cb$ and $P2_1ab$ ferroelectric phases. Experimental values estimated from Ref. 16 for the tetragonal paraelectric phase (see text) and taken from Ref. 13 for orthorhombic ferroelectric phases are reported in parentheses for comparison. We do not report Wyckoff positions for the $I4/mmm$ phase since our unit cell is doubled.

Structure	Atom	Wyckoff	x	y	z
		$I4/mmm$			
$a = 5.31$ Å	Bi		0.0000	0.5000	0.1756
(5.45)			(0.0000	0.5000	0.1701)
	W		0.0000	0.0000	0.0000
$c = 16.14$ Å	O_1		0.2500	0.7500	0.0000
(16.52)	O_2		0.0000	0.0000	0.1143
			(0.0000	0.0000	0.1152)
	O_3		0.2500	0.2500	0.7500
		$B2cb$			
$a = 5.35$ Å					
(5.49)	Bi	$8b$	0.9961	0.5149	0.1702
			(0.9947	0.5116	0.1722)
	W	$4a$	0.0000	0.0000	0.0000
$b = 5.38$ Å	AO_1	$8b$	0.2173	0.7534	0.9828
(5.52)			(0.2981	0.7399	0.9892)
	O_2	$8b$	0.0641	0.9536	0.1101
$c = 16.12$ Å			(0.0753	0.9587	0.1087)
(16.54)	O_3	$8b$	0.2369	0.2547	0.7484
			(0.2771	0.2550	0.7499)
		$P2_1ab$			
$a = 5.30$ Å	Bi_1	$4a$	0.0109	0.4843	0.1698
(5.45)			(−0.0126	0.5113	0.1730)
	Bi_2	$4a$	0.0036	0.5074	−0.1698
$b = 5.32$ Å			(−0.0113	0.4762	0.1719)
(5.48)	W	$4a$	0.0000	0.0000	0.0000
	O_1'	$4a$	0.2318	0.6896	0.0108
$c = 16.17$ Å			(0.2679	0.6933	−0.0147)
(16.47)	O_1''	$4a$	0.3321	0.1984	−0.0109
			(0.3342	0.2220	0.0163)
	O_2'	$4a$	−0.0684	−0.0368	0.1109
			(0.0854	0.0449	0.1072)
	O_2''	$4a$	0.4428	0.4563	−0.1108
			(0.5703	0.5526	−0.1086)
	O_3'	$4a$	0.2676	0.2413	0.7515
			(0.2728	0.2508	0.7489)
	O_3''	$4a$	0.2752	0.2465	0.2516
			(0.2740	0.2326	0.2514)

observed on Bi(+5e) attest to the ionico-covalent character of bonding in both the fluorite-like and the perovskite-like units of Aurivillius structures. Comparison with $A2/m$ shows that Z^* values on W along W-O chains are in the same range of values for both structures, but $O_1'(-7.76e)$ in $A2/m$ is much larger than $O_1(-4.88e)$ in $I4/mmm$.

The optical dielectric tensor ε_∞ is given by

$$\varepsilon_\infty = \begin{pmatrix} 7.60 & 0 & 0 \\ 0 & 7.60 & 0 \\ 0 & 0 & 6.84 \end{pmatrix}.$$

TABLE VI. Nonzero elements of the calculated Born effective charge tensors in Cartesian coordinates for Bi_2WO_6 in the hypothetical tetragonal $I4/mmm$ symmetry.

Atom	Z^*_{xx}	Z^*_{yy}	Z^*_{zz}	Z_{nom}
Bi	5.00	5.00	4.29	+3
W	11.09	11.09	9.32	+6
O_1	−4.88	−4.88	−1.46	−2
O_2	−2.7	−2.7	−4.74	−2
O_3	−2.95	−2.95	−2.74	−2

These values are comparable to those reported for the $A2/m$ phase.

C. Phonon instabilities

Starting from a fully relaxed tetragonal prototype structure, we computed the zone-center phonon modes of the doubled 36-atom unit cell, which, due to the folding of the Brillouin zone, in fact combine phonons at the Γ and X points in the Brillouin zone of the primitive unit cell. We identified five unstable phonon modes, twofold degenerated along the a and b directions. The mode with the largest instability lies at the Brillouin-zone center Γ with a frequency at $198i$ cm^{-1} and corresponding to the irreducible representation Γ_5^-. The four other unstable modes are at the zone boundary point $X = (\frac{1}{2},\frac{1}{2},0)$,[33] with frequencies at $183i$, $135i$, $104i$, and $98i$ cm^{-1} and corresponding to the irreducible representations, X_2^-, X_2^+, X_3^+, and X_4^+, respectively. The latter four modes are antiferrodistortive modes since they are at the zone boundary X; their condensation in the tetragonal structure will necessarily lead to the unit cell doubling along the [110] direction. The complete list of Γ phonons and a comparison with the results of Machado *et al.*[16] is provided in the Appendix.

In what follows, we describe the atomic motions associated with the different unstable modes as deduced from inspection of the real-space eigendisplacements and reported in Table VII. The strongest unstable mode Γ_5^- ($\omega = 198i$ cm^{-1}), degenerated into $\Gamma_5^-(a)$ and $\Gamma_5^-(b)$, corresponds to the polar motion of W and Bi atoms against the oxygens along the a axis for $\Gamma_5^-(a)$ or along the b axis for $\Gamma_5^-(b)$, together with a small additional shift of O_1 octahedral oxygen atoms in the ab plane.

We note that, in our calculations, only one polar mode is unstable, while the presence of a second unstable polar mode, related to a nearly rigid motion of the Bi_2O_2 layer relative to the perovskite-like block (rigid-layer mode), was reported in Ref. 16. Such a polar mode exists in our phonon calculations but appears at the slightly stable frequency of 29 cm^{-1} (labeled Γ_5^-[29] in Table VII). This difference probably arises from the slightly different cell parameters used in both calculations.

The second unstable mode, X_2^- ($\omega = 183i$ cm^{-1}), degenerated into $X_2^-(a)$ and $X_2^-(b)$, corresponds to an antipolar motion with displacements of the atoms very similar to the Γ_5^- mode, except for O_3 atoms. The third unstable mode, X_2^+ ($\omega = 135i$ cm^{-1}), degenerated into $X_2^+(a)$ and $X_2^+(b)$, consists of a rotation of oxygen octahedra about the c axis. In this mode, W and O_2 atoms have no displacements, while O_1 atoms shift

TABLE VII. Real-space eigendisplacements η of unstable and some relevant stable phonon modes of the hypothetical $I4/mmm$ structure. Eigendisplacements are normalized for the 36-atom cell according to $\langle\eta|M|\eta\rangle = 1$, with the mass matrix M in atomic mass units.[28] Internal coordinates of the different atoms are those listed in Table V. Phonon frequencies, reported in brackets, are in cm^{-1}.

	η								
Atom	x	y	z	x	y	z	x	y	z
		$\Gamma_5^-(a)$ [198i]			$X_2^-(a)$ [183i]			$X_2^+(a)$ [135i]	
Bi	0.0020	0.0000	0.0000	0.0040	0.0000	0.0000	0.0000	0.0000	0.0000
W	0.0170	0.0000	0.0000	0.0190	0.0000	0.0000	0.0000	0.0000	0.0000
O_1	−0.0400	−0.0020	0.0000	−0.0430	−0.0050	0.0000	−0.0620	−0.0620	0.0000
O_2	−0.0660	0.0000	0.0000	−0.0610	0.0000	0.0000	0.0000	0.0000	0.0000
O_3	−0.0150	0.0000	0.0000	0.0000	−0.0010	0.0000	0.0002	0.0000	0.0000
		$X_3^+(a)$ [104i]			$X_4^+(a)$ [98i]			Γ_5^- [29]	
Bi	0.0000	0.0000	0.0000	0.0000	0.0060	0.0000	0.0150	0.0000	0.0000
W	0.0000	0.0000	0.0000	0.0000	0.0000	0.0000	−0.0270	0.0000	0.0000
O_1	0.0000	0.0000	0.0470	0.0000	0.0000	−0.0510	−0.0230	−0.0010	0.0000
O_2	0.0000	0.0640	0.0000	0.0000	0.0690	0.0000	−0.0200	0.0000	0.0000
O_3	0.0000	0.0000	−0.0060	0.0000	0.0000	0.0000	0.0010	0.0000	0.0000
		X_2^- [80]			X_3^+ [107]			Γ_5^- [137]	
Bi	0.0220	0.0000	0.0000	0.0000	0.0220	0.0000	0.0010	0.0000	0.0000
W	0.0050	0.0000	0.0000	0.0000	0.0000	0.0000	−0.0040	0.0000	0.0000
O_1	−0.0300	0.0110	0.0000	0.0000	0.0000	0.0270	0.0630	0.0420	0.0000
O_2	0.0070	0.0000	0.0000	0.0000	0.0300	0.0000	−0.0420	0.0000	0.0000
O_3	0.0000	−0.0050	0.0000	0.0000	0.0000	−0.0080	−0.0130	0.0000	0.0000

in the ab plane. The difference between $X_2^+(a)$ and $X_2^+(b)$ lies in the slight motion of O_3 along the a axis for $X_2^+(a)$ or along the b axis for $X_2^+(b)$.

The fourth unstable mode, X_3^+ ($\omega = 104i$ cm^{-1}), degenerated into $X_3^+(a)$ and $X_3^+(b)$, consists essentially of a tilting of oxygen octahedra around the a axis for $X_3^+(a)$ and around the b axis for $X_3^+(b)$. In this mode there is no displacement for W atoms, while O_1 atoms move along the c axis. O_2 atoms move along the b axis for $X_3^+(a)$ or along the a axis for $X_3^+(b)$. In the Bi_2O_2 layer only O_3 atoms are moving along the c axis. The fifth unstable mode, X_4^+ ($\omega = 98i$ cm^{-1}), degenerated into $X_4^+(a)$ and $X_4^+(b)$, is very similar to X_3^+ except for the motionless O_3 atoms and the displacement of Bi atoms in the Bi_2O_2 layer.

D. Intermediate- and low-temperature phases

The condensation of these different unstable modes within the paraelectric $I4/mmm$ phase will lower the symmetry and decrease the energy. We have seen previously that the internal energy of the $I4/mmm$ phase is significantly higher than that of the $A2/m$ phase but its phonon instabilities are also about twice as large. This let us anticipate that the condensation of the latter could produce a decrease in energy one order of magnitude larger than those reported in the $A2/m$ phase[34] and so yield phases with an internal energy eventually lower that that of the $P\bar{1}$ phase discussed in the previous section. The symmetry resulting from the condensation of individual unstable modes in the $I4/mmm$ phase, together with the decrease in energy with respect to $I4/mmm$ after full atomic relaxation within this given symmetry, are reported in the top part of Table VIII. Although the different unstable modes are twofold degenerated, we restrict ourselves to the condensation of one of the two degenerated modes since other combinations do not appear in the low-symmetry phase experimentally observed that are discussed later.

The condensation of the polar $\Gamma_5^-(a)$ mode in the tetragonal paraelectric $I4/mmm$ phase distorts the structure into a ferroelectric $Fmm2$ (No. 42) phase leading, after full structural relaxation, to cell parameters $a = 5.37$ Å, $b = 5.36$ Å, and $c = 16.00$ Å. The condensation of the $X_2^-(a)$ mode leads to $Amma$ (No. 63) symmetry (conventional $CmCm$) and relaxed cell parameters $a = 5.36$ Å, $b = 5.34$ Å, and $c = 16.00$ Å. The condensation of the $X_2^+(a)$ mode leads to an orthorhombic structure, $Abam$ (No. 64) (conventional $Cmca$), with quasitetragonal cell parameters $a \approx b = 5.23$ Å and $c = 16.36$ Å. The condensation of the $X_3^+(a)$ mode leads to an orthorhombic structure, $Bmab$ (No. 64), and relaxed cell parameters $a = 5.28$ Å, $b = 5.32$ Å, and $c = 16.26$ Å. Finally, the condensation of $X_4^+(a)$ leads to $Amaa$ (No. 66) symmetry (conventional $Cccm$) and relaxed cell parameters $a = 5.28$ Å, $b = 5.31$ Å, and $c = 16.24$ Å.

We observed that, among these phases, the largest decrease in energy arises from the condensation of the largest Γ_5^- instability. The related $Fmm2$ phase does, however, still exhibit phonon instabilities.

The ferroelectric intermediate $B2cb$ phase, observed experimentally, results from the combined condensation of two unstable modes, $\Gamma_5^-(a)$ and $X_3^+(a)$, in the paraelectric $I4/mmm$ phase, while the addition of a third mode, $X_2^+(b)$, allows the ferroelectric $P2_1ab$ ground state to be reached. We notice that a proper (a) or (b) orientation of

TABLE VIII. Differences in energies with respect to the hypothetical paraelectric tetragonal $I4/mmm$ phase, ΔE_t (in meV/formula), after full structural relaxations of the different phases arising from the freezing of one or more unstable modes. The space group of each phase is given in a nonconventional setting, with c set as the long axis. Labels and frequencies ω (in cm^{-1}) of relevant phonon modes are also listed.

Mode label	ω	Symmetry	ΔE_t
Phases arising from single-mode condensation			
$\Gamma_5^-(a)$	$198i$	$Fmm2$	−114.75
$X_2^-(a)$	$183i$	$Amma$	−92.52
$X_2^+(a)$	$135i$	$Abam$	−99.63
$X_3^+(a)$	$104i$	$Bmab$	−71.01
$X_4^+(a)$	$98i$	$Amaa$	−50.04
Experimentally observed phases			
$\Gamma_5^-(a) + X_3^+(a)$		$B2cb$	−187.02
$\Gamma_5^-(a) + X_3^+(a) + X_2^+(b)$		$P2_1ab$	−216.27
Hypothetical phases			
$\Gamma_5^-(a) + X_2^+(b)$		$A2_1ma$	−206.11
$X^{3+}(a) + X^{2+}(b)$		$P2_1/a$	−105.43
$\Gamma^{5-}(a) + X^{3+}(a) + X^{2+}(a)$		Pa	−213.05
$\Gamma^{5-}(a) + X^{3+}(b) + X^{2+}(b)$		$P2_1$	−204.21

the unstable modes is necessary to match the experimental structure,[16] with a conventional a-axis direction for the polarization.

The relaxed structural parameters of the $B2cb$ and $P2_1ab$ phases are reported in Table V and show the same good agreement with experimental data as the other phases discussed previously. For the $B2cb$ phase we note that, while the LDA underestimates the lattice constants, in this case, the GGA calculation of Mohn and Stolen[17] clearly overestimates them. The related energies, with respect to the $I4/mmm$ phase, are reported in Table VIII. The lowest internal energy is associated with the $P2_1ab$ phase, which, moreover, does not exhibit any further phonon instability, in agreement with the fact that it corresponds to the experimental ground state.

We note that there are many more ways to combine unstable phonon modes than those producing the $B2cb$ and $P2_1ab$ phases and we have explored a few of them. We note, for instance, that the hypothetical $A2_1ma$ phase (No. 26) resulting from the combined condensation of the $\Gamma_5^-(a)$ and $X_2^+(b)$ modes is never observed experimentally, although it has a lower internal energy than the observed intermediate $B2cb$ phase. The decrease in energy associated with the two phases $B2cb$ and $A2_1ma$ is close to the sum of the decreases in energy obtained by each individual instability producing them, emphasizing the weak interactions between the rotations and the polar mode. On the contrary, the $P2_1/a$ phase (No. 14) arising from the condensation of $X_3^+(a)$ and $X_2^+(b)$ is much higher in energy, emphasizing the fact that both types of rotations tend to exclude each other, but not totally. Their combination with the polar mode will produce the $P2_1ab$ ground state.

In the last part of Table VIII, we also check the sensitivity of the energy to the relative orientation of the different unstable modes appearing in the $P2_1ab$ ground state. We see that replacing the $X_3^+(a)$ mode with $X_3^+(b)$ to produce a $P2_1$ phase (No. 4) has a larger effect on the energy than replacing the $X_2^+(b)$ mode with $X_2^+(a)$ to produce a Pa phase (No. 7). We note that both the $X_2^+(a)$ and the $X_2^+(b)$ modes correspond to oxygen rotations about the c axis and only differ by slight O_3 motions along either the a or the b axis.

E. Coupling of lattice modes and energy landscape

Recently, the coupling of phonon modes in perovskite compounds has received a significant renewal of interest. For instance, the trilinear coupling between polarization and two rotational modes in layered perovskite, like artificial $(SrTiO_3)/(PbTiO_3)$ superlattices[35] and natural Ruddlesden-Popper $Ca_3Ti_2O_7$ compounds,[36] has been identified as a promising road to achieve new and/or enhanced functional properties. Aurivillius phases like $SrBi_2Ta_2O_9$ are known to exhibit a similar type of trilinear coupling[3] and it is interesting to question if the same type of phenomenon is also inherent to Bi_2WO_6. In what follows, we further quantify the contributions of individual phonon modes to the different phases previously discussed in order to get a better description of the energy landscape and significant phonon couplings.

The set of phonon eigendisplacements η_i of the the $I4/mmm$ phase (normalized such that $\langle\eta|M|\eta\rangle = 1$)[27] defines a complete basis for the atomic distortions from $I4/mmm$ to a given phase, X, so that we can decompose the atomic distortion vector Δ from $I4/mmm$ to X as a sum of contributions from the different modes i:

$$\Delta = \sum_i Q_i \eta_i, \tag{3}$$

where the mode amplitude Q_i is defined as

$$Q_i = A\alpha_i = \langle\eta_i|M|\Delta\rangle. \tag{4}$$

The mode amplitude can be further decomposed into the distortion amplitude $A = \langle\Delta_i|M|\Delta\rangle$ and the cosine director α_i with respect to distortion direction η_i such that $\sum_i \alpha_i^2 = 1$. The mode amplitude Q_i quantifies which amplitude of η_i has been condensed into $I4/mmm$ to reach X, while α_i better describes

TABLE IX. Contributions α_i (see text) of the different phonon modes i to the atomic distortion from the paraelectric $I4/mmm$ phase to the different intermediate and ground-state ferroelectric phases of Bi_2WO_6. The distortion amplitude A (Bohr) is also reported in each case. Each phonon mode is identified by its symmetry label and frequency (in brackets, in cm^{-1}). The corresponding real-space eigendisplacements are reported in Table VII. We limit ourselves to contributions $\alpha_i > 0.01$.

Phase	A	Γ_5^- [198i]	X_2^- [183i]	X_2^+ [135i]	X_3^+ [104i]	X_4^+ [98i]	Γ_5^- [29]	X_2^- [80]	X_3^+ [107]	Γ_5^- [137]
Phases arising from single-mode condensation										
$Fmm2$	361.0	0.84					0.51			0.11
$Amma$	395.6		0.79					0.60		
$Abam$	444.7			0.99						
$Bmab$	444.5				0.98				0.14	
$Amaa$	384.0					0.99				
Experimentally observed phases										
$B2cb$	601.0	0.53			0.79		0.24			0.09
$P2_1ab$	582.7	0.52		0.59	0.55		0.04		0.1	0.09
Hypothetical phases										
$A2_1ma$	514.5	0.58		0.78			0.01			0.11
$P2_1/a$	455.0			0.76	0.62				0.11	

the relative contributions of the different modes entering into a given distortion.

In the top part of Table IX, we report the most significant mode contributions to the atomic distortions in the phases arising from the condensation of individual instabilities (limiting ourselves to contributions $\alpha_i > 0.01$). We can see that the $Abam$ and $Amaa$ phases arise from the condensation of the related unstable mode only, while the $Fmm2$, $Amma$, and $Bmab$ phases also involve small contributions of additional stable modes of the same symmetry, as induced by phonon-phonon anharmonic couplings.

As highlighted in the previous section, the ferroelectric $P2_1ab$ ground state results from the condensation of three distinct atomic distortions, Γ_5^-, X_3^+, and X_2^+, into $I4/mmm$. Due to symmetry considerations, these three modes cannot couple linearly. However, the Bi_2WO_6 structure does allow numerous trilinear coupling terms. Thanks to the ISOTROPY software,[33] we have identified the following symmetry-allowed possibilities involving the Γ_5^- mode and one of the X_2^+ and X_3^+ modes:

$$\Gamma_5^- \oplus X_2^+ \oplus X_3^-, \quad \Gamma_5^- \oplus X_2^+ \oplus X_4^-,$$
$$\Gamma_5^- \oplus X_3^+ \oplus X_1^-, \quad \Gamma_5^- \oplus X_3^+ \oplus X_2^-.$$

This teaches us that the presence of Γ_5^- and X_3^+ major modes in the intermediate $B2cb$ phase automatically allows the appearance of minor X_1^- and X_2^- modes. Moreover, the addition of the X_2^+ mode in the $P2_1ab$ ground state is compatible with the additional appearance of minor X_3^- and X_4^- modes. If we look in Table X, however, at the modes that have been condensed to reach the $B2cb$ and $P2_1ab$ phases, we see significant contributions only from the Γ_5^-, X_3^+, and X_2^+ modes (the unstable ones and, eventually, higher frequency modes of the same symmetries). This means that, although various trilinear coupling terms exist, none of them is strong enough to succeed in condensing any of the minor modes significantly (i.e., α_i is not rigorously 0 but is <0.01).

Since the contributions of all minor modes are negligible, we performed an expansion of the energy (in meV/formula unit), limiting ourselves to the major unstable modes that enter the observed orthorhombic phases only [i.e., $\Gamma_5^-(a)$, $X_3^+(a)$, and $X_2^+(b)$]:

$$\begin{aligned}\Delta E_i\left(Q_{\Gamma_5^-}, Q_{X_2^+}, Q_{X_3^+}\right) &= -2.50 Q_{\Gamma_5^-}^2 - 7.50\times10^{-1} Q_{X_3^+}^2 - 1.03 Q_{X_2^+}^2 \\ &+ 1.36\times10^{-5} Q_{\Gamma_5^-}^4 + 1.97\times10^{-6} Q_{X_3^+}^4 \\ &+ 2.65\times10^{-6} Q_{X_2^+}^4 + 2.10\times10^{-6} Q_{\Gamma_5^-}^2 Q_{X_3^+}^2 \\ &- 1.79\times10^{-9} Q_{\Gamma_5^-}^2 Q_{X_2^+}^2 + 1.79\times10^{-6} Q_{X_3^+}^2 Q_{X_2^+}^2.\end{aligned}$$

TABLE X. Spontaneous polarization (in $\mu C/cm^2$) of different observed or hypothetical polar phases of Bi_2WO_6. P_s(BP) refers to the polarization computed using the Berry-phase approach [Eq. (1)]. $P_s(Z^*)$ corresponds to the polarization deduced from the knowledge of the Born effective charges and atomic displacements [Eq. (2)]. The latter has been decomposed into the contributions coming from the lowest frequency Γ_5^- polar modes[37] identified by their frequency Ω (in brackets, in cm^{-1}) and mode polarity $\frac{e}{\Omega}\sum Z^*\eta$ (in parentheses, in $\mu C/cm^2$).

Phase	Γ_5^- [198i] (0.18)	Γ_5^- [29] (0.03)	Γ_5^- [137] (−0.06)	$P_s(Z^*)$	P_s(BP)
$Fmm2$	55.26	4.82	−2.40	58.59	53.98
$B2cb$	57.92	3.77	−3.30	58.29	52.06
$P2_1ab$	55.09	0.61	−3.17	52.63	48.16
$A2_1ma$	53.32	−0.13	−3.42	49.96	46.98

Q represents the mode amplitude as explained in the previous section. The values of the polynomial coefficients have been obtained by systematic energy calculations after the condensation of various combinations of the unstable modes.

The coefficients of $Q^2_{\Gamma_5^-}$, $Q^2_{X_3^+}$, and $Q^2_{X_2^+}$ are negative, coherently with the phonon instabilities. The biquadratic coupling coefficient between $\Gamma_5^-(a)$ and $X_2^+(b)$ is negative but its value is extremely small. The biquadratic coupling coefficients between $X_3^+(a)$ and both $\Gamma_5^-(a)$ and $X_2^+(b)$ are positive but still rather small, meaning that although the appearance of $X_3^+(a)$ tends to exclude the other two modes, this effect is rather small. This is confirmed by the fact that, although $\alpha_{\Gamma_5^-}$ decreases due to the appearance of the other modes, the mode amplitude $Q_{\Gamma_5^-}$ remains very similar in the $Fmm2$, $B2cb$, and $P2_1ab$ phases.

The coupling scenario in Bi_2WO_6 is therefore rather different from those of other previously studied Aurivillius phases, namely, $SrBi_2Ta_2O_9$ ($m = 2$) and $Bi_4Ti_3O_{12}$ ($m = 3$). In $SrBi_2Ta_2O_9$, the strongest instability is the octahedral tilting mode X_3^- around the a/b direction, and the condensation of this mode alone results in a nonpolar intermediate phase. This tilting mode and the polar mode Γ_5^- are mutually exclusive, and the final ferroelectric phase $Ama2_1$ requires the presence of a third stable mode, X_2^+, to stabilize.[3] In $Bi_4Ti_3O_{12}$, as for Bi_2WO_6, there are three major unstable modes, Γ_5^-, X_2^+, and X_3^+. However, there is no occurrence of experimentally detected intermediate phases, and the ferroelectric $B1a1$ monoclinic ground state is reached by the simultaneous condensation of the three unstable modes and could be denoted as an avalanche phase transition.[4]

F. Spontaneous polarization

In both orthorhombic ferroelectric phases, spontaneous polarization P_s expands along the a direction only, with no component along c. We report, in Table X, the spontaneous polarizations of different observed and hypothetical phases as obtained using the Berry-phase approach [P_s(BP)] and using Eq. (2) and the knowledge of the Born effective charges and atomic distortions [$P_s(Z^*)$]. Again, determination of P_s(BP) requires careful determination of the polarization quantum (see discussion in Sec. III D).

In Table X we also report the contributions to the full polarization arising from the individual Γ_5^- polar modes. We see that the main contribution arises from the unstable Γ_5^- mode, which is also the most polar. We observe that the spontaneous polarization is rather constant in the different phases, in agreement with the weak coupling between polar and rotational modes, yielding an almost-constant amplitude of $Q_{\Gamma_5^-}$ as discussed in the previous section. The polar mode of the highest frequency makes a tiny contribution but tends to reduce the full polarization. We note that $P_s(Z^*)$ slightly overestimates P_s(BP), but since the same distortion is used in both approaches, this has to be linked to the evolution of the Born effective charges along the path of atomic distortion and neglected in the computation of $P_s(Z^*)$.

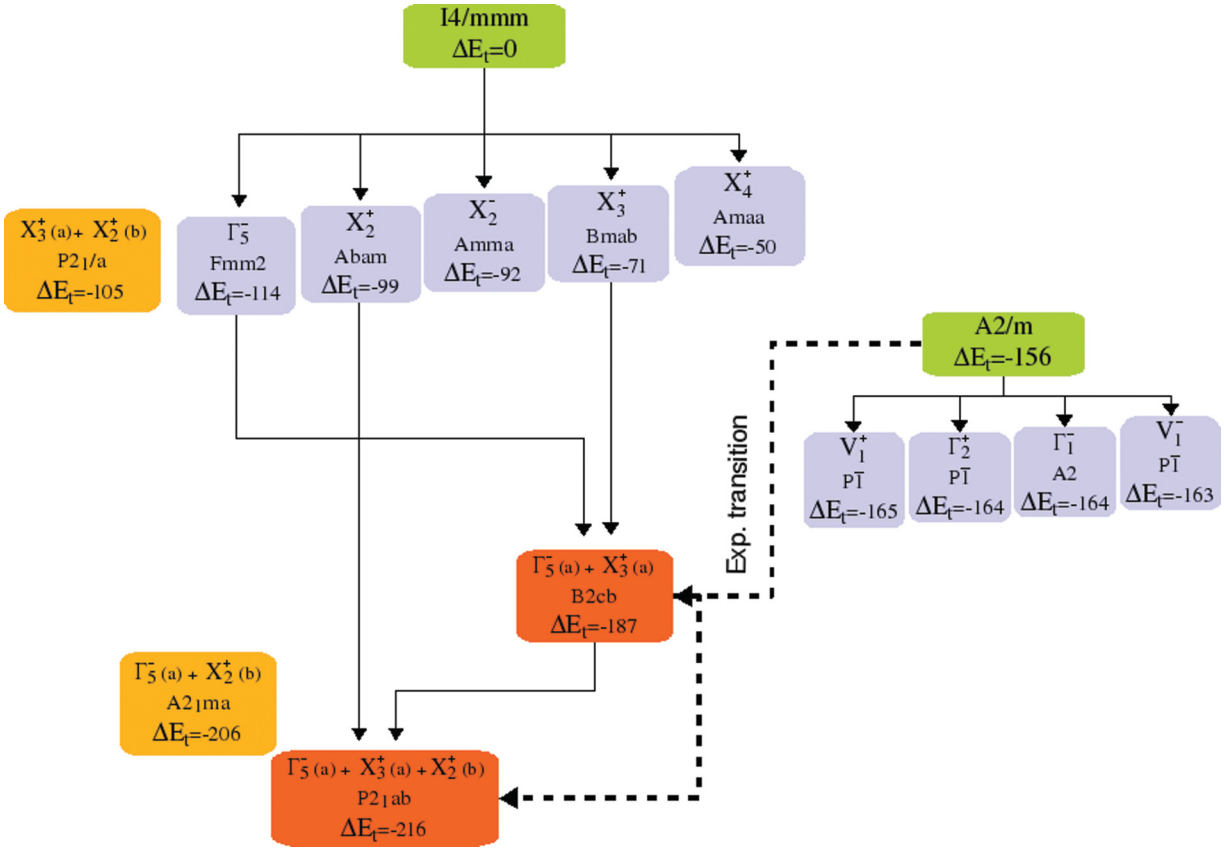

FIG. 4. (Color online) Summary diagram of phase transitions in Bi_2WO_6. ΔE_t is in meV/formula unit and represents the difference in energy with respect to $I4/mmm$, taken as the zero-energy reference.

Independently, we also decomposed the polarization in terms of contributions coming from the individual layers: the main contribution (76% of the total polarization) comes from the perovskite-like block, due to the displacement of W opposite its surrounding octahedral oxygen atoms O_1 and O_2, while a smaller part (24% of the total polarization) comes from the Bi_2O_2 layer, due to Bi displacement opposite O_3. This means that the contribution of Bi_2O_2 to the polarization is not dominant, contrary to the usual belief.[6]

V. DISCUSSION

In the previous sections, we have discussed many different phases of Bi_2WO_6. In Fig. 4, we provide a summary comparing the internal energies of all the phases we have studied. This diagram gives a global view and helps clarify the phase transitions.

At high temperatures Bi_2WO_6 crystallizes in a monoclinic $A2/m$ structure. Starting from this configuration, displacive phase transitions to $A2$ or $P\bar{1}$ phases are possible. However, Bi_2WO_6 can adopt another polymorphic $I4/mmm$ tetragonal form, which displays much stronger phonon instabilities, yielding orthorhombic $B2cb$ and $P2_1ab$ phases of lower energies. Starting at high temperatures from the $A2/m$ structure, the system has to exhibit a reconstructive phase transition to reach the $P2_1ab$ ground state.

VI. CONCLUSIONS

We have performed a first-principles study of Bi_2WO_6 using density functional theory within the LDA. First, we characterized the high-temperature paraelectric monoclinic $A2/m$ phase. Phonon frequencies and dielectric properties were computed. This monoclinic structure, with a configuration mixing edge-sharing and corner-sharing $(WO_4)^{-2}$ octahedra, exhibits, as in typical perovskites, anomalous Z^* values on W and its surrounding oxygens along the corner-sharing chains, potentially yielding a non-negligible spontaneous polarization along this direction. A lattice dynamics study reveals four structural instabilities that lead the system to energetically quasiequivalent monoclinic phases. One of these phases is ferroelectric, with space group $A2$ and a spontaneous polarization of 20 $\mu C/cm^2$.

Second, we considered a hypothetical paraelectric $I4/mmm$ phase that, although not observed experimentally, has a symmetry that is the supergroup of the low-temperature orthorhombic phases observed experimentally. We fully characterized the $I4/mmm$ phase, which exhibits five degenerated phonon instabilities. Our calculations agree with the observation that Bi_2WO_6 has a $P2_1ab$ ground-state structure. This ground state can be reached from the condensation of three unstable phonons in the paraelectric $I4/mmm$ phase: a polar mode, Γ_5^-; a rotation of oxygen octahedra around the c axis, X_2^+; and a tilt of oxygen octahedra around the a axis, X_3^+. The experimentally observed $B2cb$ phase appears as an intermediate phase along this path, arising from the condensation of the Γ_5^- and X_3^+ modes. Our calculations reveal a weak coupling between the different modes entering the ground state and the absence of significant distortion arising from minor modes allowed by symmetry. As in other perovskite ferroelectric oxides, the Z^* values are anomalously large, yielding the strong spontaneous polarization of 48 $\mu C/cm^2$ in the $P2_1ab$ phase. The significantly lower internal energy of the $P2_1ab$ phase, compared to the $P\bar{1}$ phase, is in agreement with the fact that, starting from $A2/m$ phase, the system displays a reconstructive phase transition.

ACKNOWLEDGMENTS

This work was performed during a visit by H.D. to the University of Liège in Belgium, with the combined support of the Algerian Ministry of High Education and Scientific Research (MESRS) and the Interuniversity Attractive Pole Program of the Federal Science Research Policy of Belgium. P.G. thanks the Francqui Foundation for a Research Professorship. E.B. thanks the FRS-FNRS Belgium.

APPENDIX

In this Appendix we report, for completeness, the full set of Γ phonons in the $A2/m$ (see Table XI) and $I4/mmm$ (see Table XII) phases of Bi_2WO_6 as computed within the LDA in the fully relaxed structures. For the $A2/m$ phases no previous calculations have been reported and no experimental data are available. Our results therefore constitute a theoretical prediction that might be useful for interpretation of future experimental measurements. For the hypothetical $I4/mmm$ phase, our results are compared to those of Machado *et al.*[16] also within the LDA but at a larger volume. As usual in ferroelectric oxides, the use of a larger volume favors ferroelectric instability.

TABLE XI. Frequencies (in cm^{-1}) of phonon modes at Γ in the monoclinic $A2/m$ phase of Bi_2WO_6.

Γ_1^- (A_u)	Γ_1^+ (A_g)	Γ_2^- (B_u)	Γ_2^+ (B_g)
108*i*	87	54	63*i*
61	91	82	178
278	122	96	241
295	160	144	303
336	167	194	378
408	192	209	455
653	272	280	456
654	298	309	
	333	352	
	380	353	
	404	358	
	441	444	
	468	473	
	497	624	
	642	787	
	663	876	
	665		
	750		
	895		

TABLE XII. Frequencies (in cm^{-1}) of phonon modes at Γ in the tetragonal $I4/mmm$ phase of Bi_2WO_6. Values in brackets are those reported in Ref. 16.

Γ_5^- (E_u)	Γ_5^- (E_u)[16]	Γ_5^+ (E_g)	Γ_3^- (A_{2u})	Γ_3^- (A_{2u})[16]	Γ_1^+ (A_{1g})	Γ_4^- (B_{2u})	Γ_2^+ (B_{1g})
198i	(271i)	71	89	(51)	176	312	437
29	(34i)	281	348	(337)	767		
137	(133)	517	469	(437)			
359	(211)		674	(630)			
650	(525)						

*Corresponding author: hdjani@ulg.ac.be

[1] B. Aurivillius, Arkiv for Kemmi **1**, 463 (1949).

[2] I. Etxebarria, J. M. Perez-Mato, and P. Boullay, Ferroelectrics **401**, 17 (2010).

[3] J. M. Perez-Mato, M. Aroyo, A. Garcia, P. Blaha, K. Schwarz, J. Schweifer, and K. Parlinski, Phys. Rev. B **70**, 214111 (2004).

[4] J. M. Perez-Mato, P. Blaha, K. Schwarz, M. Aroyo, D. Orobengoa, I. Etxebarria, and A. Garcia, Phys. Rev. B **77**, 184104 (2008).

[5] C. H. Hervoches, A. Snedden, R. Riggs, S. H. Kilcoyne, P. Manuel, and P. Lightfoot, J. Solid State Chem. **164**, 280 (2002).

[6] R. L. Withers, J. G. Thompson, and A. D. Rae, J. Solid State Chem. **94**, 404 (1991).

[7] E. C. Subbarao, J. Phys. Chem. Solids **23**, 665 (1962).

[8] G. A. Smolenskii, V. A. Isupov, and A. I. Agranovskaya, Sov. Phys. Solid State **3**, 651 (1961).

[9] C. A. Paz de Araujo, J. D. Cuchlaro, L. D. McMillan, M. C. Scott, and J. F. Scott, Nature (London) **374**, 627 (1995).

[10] Y. Li, J. Liu, X. Huang, and G. Li, Cryst. Growth Des. **7**, 1350 (2007).

[11] N. Kim, R. N. Vannier, and C. P. Grey, Chem. Mater. **17**, 1952 (2005).

[12] A. Kudo and S. Hijii, Chem. Lett. **1999**, 1103 (1999).

[13] N. A. McDowell, K. S. Knight, and P. Lightfoot, Chem. Eur. J. **12**, 1493 (2006).

[14] H. Kodama and A. Watanabe, J. Solid State Chem. **56**, 225 (1985).

[15] G. Sankar, M. A. Roberts, J. M. Thomas, G. U. Kulkarni, N. Rangavittal, and C. N. R. Rao, J. Solid State Chem. **119**, 210 (1995).

[16] R. Machado, M. G. Stachiotti, R. L. Migoni, and A. H. Tera, Phys. Rev. B **70**, 214112 (2004).

[17] C. E. Mohn and S. Stolen, Phys. Rev. B **83**, 014103 (2011).

[18] P. Hohenberg and W. Kohn, Phys. Rev. B **136**, 864B (1964).

[19] W. Kohn and L. J. Sham, Phys. Rev. B **140**, 1133A (1965).

[20] X. Gonze, J.-M. Beuken, R. Caracas, F. Detraux, M. Fuchs, G.-M. Rignanese, L. Sindic, M. Verstraete, G. Zerah, F. Jollet, M. Torrent, A. Roy, M. Mikami, P. Ghosez, J.-Y. Raty, and D. C. Allan, Comput. Mater. Sci. **25**, 478 (2002).

[21] X. Gonze, G.-M. Rignanese, M. Verstraete, J.-M. Beuken, Y. Pouillon, R. Caracas, F. Jollet, M. Torrent, G. Zerah, M. Mikami, P. Ghosez, M. Veithen, V. Olevano, L. Reining, R. Godby, G. Onida, D. Hamann, and D. C. Allan, Z. Kristallogr. **220**, 558 (2005).

[22] X. Gonze *et al.*, Comput. Phys. Commun. **180**, 2582 (2009).

[23] J. P. Perdew and Y. Wang, Phys. Rev. B **45**, 13244 (1992).

[24] M. P. Teter, Phys. Rev. B **48**, 5031 (1993).

[25] H. J. Monkhorst and J. D. Pack, Phys. Rev. B **13**, 5188 (1976).

[26] H. B. Schlegel, J. Comput. Chem. **3**, 214 (1982).

[27] X. Gonze and C. Lee, Phys. Rev. B **55**, 10355 (1997).

[28] Real-space eigendisplacements η are related to the dynamical matrix eigenvectors γ through $\eta_{\kappa,\alpha} = \gamma_{\kappa,\alpha}/\sqrt{(M_\kappa)}$, where κ runs over all the atoms, α runs over the three directions, and M_κ is the mass of atom κ. Since dynamical matrix eigenvectors are normalized as $\langle\gamma|\gamma\rangle = \sum_{\kappa,\alpha} \gamma^*_{\kappa,\alpha}\gamma_{\kappa,\alpha} = 1$, the related eigendisplacements are normalized as $\langle\eta|M|\eta\rangle = \sum_{\kappa,\alpha} M_\kappa \eta^*_{\kappa,\alpha}\eta_{\kappa,\alpha} = 1$, where M is the mass matrix.[27,38]

[29] R. Resta, Rev. Mod. Phys. **66**, 899 (1994).

[30] P. Ghosez, J.-P. Michenaud, and X. Gonze, Phys. Rev. B **58**, 6224 (1998).

[31] F. Detraux, P. Ghosez and X. Gonze, Phys. Rev. B **56**, 983 (1997).

[32] S. C. Miller and W. F. Love, *Tables of Irreducible Representations of Space Group and Co-representations of Magnetique Space Groups* (University of Colorado Press, Boulder, 1967).

[33] This unusual notation of X is that used in the ISOTROPY program package (H. T. Stokes, D. M. Hatch, and B. J. Campbell, 2007; stokes.byu.edu/isotropy.html) and in the SYMMODES program of the Bilbao Crystallographic Server (http://www.cryst.ehu.es), where $X = (0,0,\frac{1}{2})$ is taken in the reciprocal basis of the primitive unit cell and $X = (\frac{1}{2},\frac{1}{2},0)$ in the reciprocal basis of the conventional centered cell.

[34] Assuming a double-well internal energy, related to the ionic degrees of freedom Q and the unstable phonon frequency ωi, of the form $E = (-1/2)\omega^2 Q^2 + (1/4)\beta Q^4$, the well depth is $\Delta E = \omega^4/4\beta$. So, increasing the amplitude of the instability ω by a factor of 2 will increase the well depth by a factor of 16 (assuming the anharmonic coefficient is unchanged).

[35] E. Bousquet, M. Dawber, N. Stucki, C. Lichtensteiger, P. Hermet, S. Gariglio, J.-M. Triscone, and P. Ghosez, Nature (London) **452**, 732 (2008).

[36] N. A. Benedek and C. J. Fennie, Phys. Rev. Lett. **106**, 107204 (2011).

[37] Contributions from other polar modes are not reported.

[38] P. Ghosez, Ph.D. thesis, Université Catholique de Louvain, 1997.